THE JOURNAL OF PHYSICAL CHEMISTRY C
A JOURNAL OF THE AMERICAN CHEMICAL SOCIETY

pubs.acs.org/JPCC

Article

Calcite/Aragonite Epitaxy: A Computational Study for Understanding Mollusk Shell Formation

Marco Bruno,* Mauro Prencipe, Dino Aquilano, Andrea Cotellucci, Stefano Ghignone, and Péter Németh

Cite This: *J. Phys. Chem. C* 2022, 126, 6472−6481

Read Online

ACCESS | Metrics & More | Article Recommendations | Supporting Information

ABSTRACT: Understanding the selection mechanisms of $CaCO_3$ polymorphs (vaterite, aragonite, and calcite) is pivotal for elucidating both inorganic and biogenic carbonate formation. It is peculiar that different polymorphs originate from the same organism; in addition, these polymorphs can even be epitaxially related. Here, we ask why some mollusks and gastropods develop calcite (Cc) layers at the contact with aragonite (Ar) in the outer portion of their shell, while others do not. To establish the most likely epitaxial relationships between calcite and aragonite, here, we investigated at the empirical level (and 0 K) the $(001)_{Ar}/(00.1)_{Cc}$, $(110)_{Ar}/(10.0)_{Cc}$, $(010)_{Ar}/(01.2)_{Cc}$, and $(100)_{Ar}/(11.0)_{Cc}$ interfaces. Upon analyzing the $(001)_{Ar}/(00.1)_{Cc}$ epitaxial and relaxed interface, we found that a hexagonal (space group, $P6_322$) $CaCO_3$ polymorph is generated, corresponding to the phase recently identified during the molecular dynamics study on the high-temperature (~600 K) aragonite−calcite transition. This polymorph, showing a symmetric intermediate between aragonite (orthorhombic) and calcite (rhombohedral), develops as a nanometric phase and exhaustively explains the observed epitaxy, $(001)_{Ar}/(00.1)_{Cc}$. We propose that the growth of calcite at room pressure and temperature in the outer portion of the shell of mollusks and gastropods is strictly associated with the formation of this hexagonal $CaCO_3$ polymorph. Moreover, to intensify the growth process of carbonate polymorphs, we can envisage that the findings have implications for understanding the sluggish mechanisms of aragonite−calcite transformation under ambient conditions.

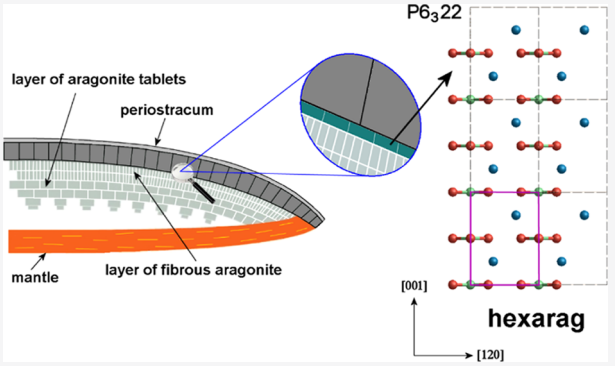

1. INTRODUCTION

Aragonite is a $CaCO_3$ polymorph, stable at high pressure and metastable at room pressure. The transformation of aragonite (Ar) into calcite (Cc) represents a long-standing debate. In the initial stages of this kind of research, experiments concerned the Ar ↔ Cc transition, achieved by heating in the range 390−490 °C, and investigated by means of differential thermal analysis (DTA) measurements and X-ray powder diffraction (XRPD) measurements. From DTA it appeared evident that the smallness of the first endothermic peak indicates that only a small amount of energy is needed for the aragonite → calcite transformation.[1−3] Moreover, Kleber,[4] examining this transformation by X-ray, found polycrystalline aggregates of calcite (instead of preferentially oriented crystals) appearing when aragonite was heated to 400 °C. Successively Dasgupta,[5] studied the behavior of a single crystal of aragonite heated at 400 °C and proposed that the Ar → Cc transition would be an oriented and topotactic one. As a matter of fact, the orientational relationship is such that the directions of *c*-axes of the two phases coincide, being $[001]_{Ar}/[001]_{Cc}$, while, in the basal plane they are $[100]_{Ar}/[10.0]_{Cc}$ and $[110]_{Ar}/[01.0]_{Cc}$. The kinetics of the Ar−Cc transformation in aqueous solution were investigated by X-ray diffraction to determine factors involved in the process of calcite formation and the controlling diagenetic conditions for the transformation.[6] The crystallization of calcite from the aragonite crystal seeds was carried out at 108 °C. At this temperature, the reaction required from 12 h to one week for completion (depending on the solution); at room temperature and pressure, the reaction would require from months to years to complete.[6] From a careful interpretation of reaction kinetics it follows that calcite nucleation is neither homogeneous nor induced on free particles in solution or on glass walls, but occurs on aragonite surfaces, whereas growth takes place on point or line defects. Nucleation and growth of aragonite on calcite, along with the topotactic Ar−Cc transformation have been investigated as well owing to metamorphic implications.[7,8] Good papers were published as well, concerning the topotactic

Received: February 1, 2022
Revised: March 7, 2022
Published: March 30, 2022

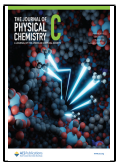

https://doi.org/10.1021/acs.jpcc.2c00785
J. Phys. Chem. C 2022, 126, 6472−6481

relationships and the role played by the dislocations.[9,10] Geological environment is specially concerned with the Ar−Cc transitions, occurring both in sedimentary rocks and in speleothems. The transmission electron microscopy (TEM) investigation of these samples provides insights into the replacement mechanism. In particular, it shows that recrystallization occurs primarily along crystal defects, suggesting that the kinetics of the replacement are controlled mainly by the microstructure of aragonite at least under conditions of slow diagenetic alteration.[11] The replacive calcite in the San Cassiano fossils and the calcite crystals of the cement display a pervasive, modulated microstructure when observed by TEM.[11] This observation can be attributed either to compositional variations (Mg and Fe containing calcite), stacking disorder, or positional disorder of anions. Calcite nanocrystalline aggregates and single crystals are found in Triassic shallow marine facies, which are famous for their preservation of original aragonite, influenced by the continental siliciclastic input.[12] The aragonite−calcite problem reached a relevant complexity from the very first steps of the biomineralization.[13] In many living systems, it is common to observe the contemporary presence of aragonite and calcite in a quasi-epitaxial relationship. An interesting and widely known example of this association is the shell of some mollusks and gastropods. From the inside to the outside of the shell, one observes: (i) a nacreous layer composed of thin aragonite (001) hexagonal tablets intercalated with interlamellar organic sheets, with the *c*-axis of the tablets perpendicular to the lamination of nacre;[14] (ii) a fibrous layer composed of horn-like aragonite crystals, in which the upper part of the layer, the *c*-axis of the aragonite crystals is oriented perpendicular to the shell surface;[15,16] and (iii) prismatic calcite layers.[17]

The current but qualitative interpretation of all phenomena concerning the findings of the coexisting calcite and aragonite (either in mutual physical contact or not) is that calcite and aragonite crystals are epitaxially related, taking advantage of the hypothesized high adhesion energy, β_{adh}, between the two phases, where β_{adh} is the energy released when two separated phases are placed in contact. However, quantitative evaluations of the possible epitaxial relationships have not yet been obtained.

Taking a cue from the just mentioned and most relevant paper[9] dealing with the Ar ↔ Cc topotaxies, in this paper we aim at investigating the following epitaxies: $(001)_{Ar}/(00.1)_{Cc}$, $(110)_{Ar}/(10.0)_{Cc}$, $(010)_{Ar}/(01.2)_{Cc}$, and $(100)_{Ar}/(11.0)_{Cc}$ to find, which of these couplings can be associated with two-dimensional (2D)-lattice coincidences fulfilling the epitaxial constraints. Anyhow, it should be kept in mind that in the following it was adopted that calcite is the substrate and aragonite represents the deposit standing on it. Moreover, both specific adhesion β_{adh} and interface γ_{int} (erg cm^{-2}) energies will be calculated for each of the allowed epitaxies, where γ_{int} is the energy amount needed to increase the interface of a unit area.

2. COMPUTATIONAL METHODS

To establish the most likely epitaxial relationships between calcite and aragonite, here, we investigated, at the empirical level, the just quoted epi-interfaces determining both their structures and thermodynamic properties at 0 K. A composed slab, $(hkl)_{Ar}/(h'k'.l')_{Cc}$, made from aragonite and calcite (slab Ar and slab Cc hereinafter), was generated in the following way:[18,19] (i) we searched for the two-dimensional (2D) coincidence lattices between the two phases in an epitaxial relationship at the reticular level (which will be discussed in the following paragraphs) and, successively, we considered only those fulfilling the rigorous epitaxial constraints; (ii) the Ar and Cc slabs of a selected thickness were made by cutting their respective bulk structures parallel to the lattice planes of interest and using the same 2D-cell parameters describing the epitaxy; (iii) slab Ar was placed above slab Cc; and (iv) finally, the composed slab structures (atomic coordinates and 2D-cell parameters) were optimized by considering all of the atoms free to move.

Structure optimization of the $(001)_{Ar}/(00.1)_{Cc}$, $(110)_{Ar}/(10.0)_{Cc}$, $(010)_{Ar}/(01.2)_{Cc}$, and $(100)_{Ar}/(11.0)_{Cc}$ composed slabs was performed at the empirical level using the calcium carbonate minerals force field developed by Rohl et al.,[20] and version 4.0 of the GULP simulation code.[21] The computational parameters adopted in our calculations are suitable to guarantee convergence on the energy values discussed in the main text, as well as the thickness of the composed slabs. GULP output files, listing the optimized fractional coordinates and optimized 2D-cell parameters of the composed slabs, are freely available at http://mabruno.weebly.com/download. We only performed static calculations at 0 K, the vibrational entropy and energies were not calculated. However, as discussed in our previous works,[22,23] neglecting the vibrational contribution should not lead to a significant error in the estimate of the adhesion and interfacial energies. A detailed description of the computational methodology adopted for the study of interfaces is reported in the paper by Bruno et al.[19]

The adhesion energy (erg cm^{-2}) reads

$$\beta_{adh}^{(hkl)_{Ar}/(h'k'.l')_{Cc}} = \frac{E_{(h'k'.l')}^{Cc} + E_{(hkl)}^{Ar} - E_{(hkl)/(h'k'.l')}^{Ar/Cc}}{S} \quad (1)$$

where $E_{(hkl)/(h'k'.l')}^{Ar/Cc}$, $E_{(h'k'.l')}^{Cc}$, and $E_{(hkl)}^{Ar}$ represent the energies of the $(hkl)_{Ar}/(h'k'.l')_{Cc}$ composed slab, isolated $(h'k'.l')_{Cc}$ slab and isolated $(hkl)_{Ar}$ slab, respectively, and S is the area of the 2D-coincidence cell. Adhesion energy is intimately related to the interface energy, $\gamma_{int}^{(hkl)_{Ar}/(h'k'.l')_{Cc}}$ (erg cm^{-2}) by the Young−Dupré's relation[24]

$$\gamma_{int}^{(hkl)_{Ar}/(h'k'.l')_{Cc}} = \gamma_{(h'k'.l')}^{Cc} + \gamma_{(hkl)}^{Ar} - \beta_{adh}^{(hkl)_{Ar}/(h'k'.l')_{Cc}} \quad (2)$$

where $\gamma_{(h'k'.l')}^{Cc}$ and $\gamma_{(hkl)}^{Ar}$ are the specific surface energies, in a vacuum, of the $(h'k'.l')$ and (hkl) faces of calcite and aragonite, respectively.

It should be outlined here once again that ref 24 has been cited because Young−Dupré's relation fixed the conditions for growing the deposit (aragonite) on the substrate (calcite)

(i) if $\beta_{adh}^{(hkl)_{Ar}/(h'k'.l')_{Cc}} < 2\gamma_{(hkl)}^{Ar}$, three-dimensional (3D) aragonite can grow on calcite in solutions supersaturated with respect to aragonite;

(ii) if $\beta_{adh}^{(hkl)_{Ar}/(h'k'.l')_{Cc}} = 2\gamma_{(hkl)}^{Ar}$, then aragonite assumes a monomolecular thickness on the calcitic substrate;

(iii) finally, if $\beta_{adh}^{(hkl)_{Ar}/(h'k'.l')_{Cc}} > 2\gamma_{(hkl)}^{Ar}$, 2D-aragonite crystals can spontaneously grow on calcite in solutions unsaturated with respect to aragonite.

3. RESULTS AND DISCUSSION

The lattice spacings, corresponding to the couplings $(001)_{Ar}/(00.1)_{Cc}$, $(110)_{Ar}/(10.0)_{Cc}$, $(010)_{Ar}/(01.2)_{Cc}$, and $(100)_{Ar}/(11.0)_{Cc}$ are listed in Table 1.

Our first step is to search for epitaxies, if any, that might occur at the just quoted interfaces. Accordingly, one has to determine the corresponding 2D-lattice coincidences, along with their 2D meshes. The following cell parameters (Å) have been adopted:

https://doi.org/10.1021/acs.jpcc.2c00785
J. Phys. Chem. C 2022, 126, 6472−6481

Table 1. Interplanar Spacings (Å) Corresponding to the Couplings $(001)_{Ar}/(00.1)_{Cc}$, $(110)_{Ar}/(10.0)_{Cc}$, $(010)_{Ar}/(01.2)_{Cc}$, and $(100)_{Ar}/(11.0)_{Cc}$[a]

aragonite	calcite	Δ%
$d_{002} = 2.8704$	$d_{00.6} = 2.8433$	−0.95
$d_{110} = 4.2114$	$3 \times d_{30.0} = 4.3211$	+2.6
$d_{020} = 3.9856$	$d_{01.2} = 3.8548$	−3.34
$d_{200} = 2.4805$	$d_{11.0} = 2.4948$	+0.57

[a]Percent misfits, Δ%, represents the quality of the facing lattice spacings.

(i) calcite ($R\bar{3}c$): $a_0 = b_0 = 4.9896$; $c_0 = 17.06$; $\alpha = \beta = 90°$ and $\gamma = 120°$; aragonite ($Pmcn$): $a_0 = 4.9611$; $b_0 = 7.9672$; $c_0 = 5.7407$; $\alpha = \beta = \gamma = 90°$ (Table 2). It is worth remembering that all of the 2D cells of the lattice planes involved except for the $(00.1)_{Cc}$ plane are rectangular.

Table 2. Vectors (Å) of the 2D Cells That Can be Found in the Lattice Planes Involved in the Epitaxies $(001)_{Ar}/(00.1)_{Cc}$, $(110)_{Ar}/(10.0)_{Cc}$, $(010)_{Ar}/(01.2)_{Cc}$, and $(100)_{Ar}/(11.0)_{Cc}$

	aragonite	calcite
lattice planes	001	00.1
vectors (Å) of the 2D cells	[100] = 4.9611	[100] = 4.9896
	[010] = 7.9672	[010] = 4.9896
	110	10.0
	$[1\bar{1}0] = 9.3855$	[010] = 4.9896
	[001] = 5.7407	[001] = 17.06
	010	01.2
	[100] = 4.9611	[100] = 4.9896
	[001] = 5.7407	$1/3[12\bar{1}] = 6.38$
	100	11.0
	[010] = 7.9672	$[1\bar{1}0] = 8.6422$
	[001] = 5.7407	[001] = 17.06

Thus, we will analyze in detail both the reticular and energetic conditions connected to each of the couplings described in Tables 1 and 2, to check whether the conditions for the existence of epitaxy are met. To do that, the theoretical surface profiles of the faces involved in the epitaxies are needed. To this end, the best approach is the rigorous application of the morphological method of Hartman−Perdok.[25]

3.1. Aragonite (001)/Calcite (00.1) Epitaxy. The $\{001\}_{Ar}$ pinacoid has been studied first by Heijnen[26] and, successively, by our research team.[27,28] Its character is flat (F), the allowed slice thickness is d_{002}, and outermost surface layer can be terminated either by Ca^{2+} or CO_3^{2-} ions. Here, we will deal only with the most stable surface profile which is CO_3^{2-} terminated. Its surface-specific energy value is 779 erg cm^{-2}.

Since the good paper by Heijnen,[29] the $\{001\}_{Cc}$ pinacoid has been extensively studied because calcite is not only the most celebrated crystal from the historical point of view but, owing to its complex and strongly anisotropic structure, also is of more and more increasing importance in both inorganic and biological systems. As an example, the surface structure of the $\{00.1\}_{Cc}$ form seems to offer the most suitable interface for the preparation of different organic/inorganic monolayer systems in biomineralization processes. $\{00.1\}_{Cc}$ is a kinked (K) form; its d_{006} slices, allowed by the $R\bar{3}c$ space group, are made of alternating layers of Ca^{2+} and CO_3^{2-} ions, as it appears when the structure is observed along any direction perpendicular to the [001] triad axis. Consequently, the ideal {00.1} form exhibits iso-oriented dipoles in its outermost layers, and hence, it shows unstable terminations that need to be reconstructed. There are two allowed ways of reconstructing: in one of them (R1), one half of the outmost charged layer is removed while, in the other (R2), the outmost d_{006} slice undergoes an octopolar scheme, which obeys the bulk crystal symmetry. Accordingly, four reconstructions can be made due to duplicity of the ionic terminations.[30]

In Table 3, the main 2D-coincidence lattices considered to describe the $(001)_{Ar}/(00.1)_{Cc}$ epitaxy are listed. Complete description of 2D-coincidence lattices can be seen in Table S1 (Supporting Information). The rotation angle indicates the anticlockwise angle between the vectors $[010]_{Ar}$ and $[010]_{Cc}$. Ranking increases with the size of the 2D-supercell area.

Cases (1a) and (1b) have the same area misfit. Actually, their area misfit is close to the limiting condition so a good epitaxy can occur. Nevertheless, in our geometrical coincidences, the surface relaxation is not taken into account, for both aragonite and calcite lattices. Moreover, it is necessary to remember that the coincidence supercells (1a) and (1b) are symmetry equivalent since they are mutually rotated by 60°, according to the trigonal symmetry of the (00.1) plane of calcite. This is the reason why the area misfit (−9.096%) is the same in (1a) and (1b).

A further consideration applies to the peculiarity of the $(001)_{Ar}/(00.1)_{Cc}$ epitaxy. Ranking (1a) shows the smallest coincidence supercell fulfilling the epitaxial constraints; this is a rectangular supercell, as illustrated in Figure 1. In the same figure, one can find the pseudohexagonal supercell corresponding to ranking (1b). Finally, we wanted to emphasize the pseudohexagonality of the epitaxial interface only because this reticular property is premonitory of the spontaneous appearance of a new hexagonal nanophase occurring at room temperature in the epitaxial transition between the orthorhombic aragonite (001) and the rhombohedric calcite (00.1). In the following section, we will deal in detail with the physical aspects of this transition.

Table 3. Main 2D-Coincidence Lattices Describing the $(001)_{Ar}/(00.1)_{Cc}$ Epitaxy. The Rotation Angle Indicates the Anticlockwise Angle between the Vectors $[010]_{Ar}$ and $[010]_{Cc}$

		$(00.1)_{Cc}$	$(001)_{Ar}$	linear and area misfit (Δ%)	rotation angle (deg)
	ranking				
2D-cell corresponding lattice vectors (Å)	(1a)	[010] = 4.9896	[100] = 4.9611	−0.574	90
		[210] = 8.6422	$[0\bar{1}0] = 7.9672$	−8.47	
2D-supercell area (Å^2) and multiplicity		43.121 (2×)	39.526 (1×)	−9.096	
2D-cell corresponding lattice vectors (Å)	(1b)	2[100] = 9.9792	$[1\bar{1}0] = 9.3855$	−6.325	30
		2[110] = 9.9792	2[100] = 9.9222	−0.574	
2D-supercell area (Å^2) and multiplicity		86.242 (4×)	79.052 (2×)	−9.096	

https://doi.org/10.1021/acs.jpcc.2c00785
J. Phys. Chem. C 2022, 126, 6472−6481

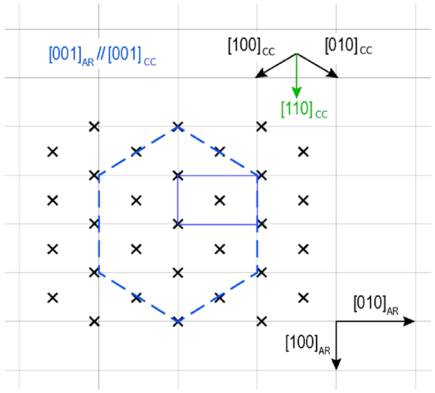

Figure 1. Lattices of aragonite and calcite viewed along their common direction [001] ≡ *z*-axis. The smallest rectangular 2D cell (solid lines) and pseudohexagonal 2D-supercell are outlined (dashed lines), where the $[110]_{Cc}$ direction coincides with the $[100]_{Ar}$ direction. See ranking (1a) and (1b) in Table 3.

3.1.1. Energetics of the $(001)_{Ar}/(00.1)_{Cc}$ Epitaxy. For the {001} aragonite pinacoid, we choose the CO_3-terminated outmost layer, $(001)^{Ar}_{CO_3}$, since its surface energy value is by far lower than those of the Ca-terminated layer.[28] In Table 4, the two possible interfacial energies of the epitaxy are indicated: $(001)^{Ar}_{CO_3}$ was placed in contact with two terminations of the (00.1) surface of calcite: Ca-terminated, $(00.1)^{Cc}_{Ca}$, and CO_3-terminated, $(00.1)^{Cc}_{CO_3}$; R1 reconstruction was adopted for both the calcite terminations. Surface relaxation has been taken into account and 2D cell (1b) (Table 3) has been adopted for energy calculations.

Table 4. Adhesion ($\beta^{(001)_{Ar}/(00.1)_{Cc}}_{adh}$) and Interface ($\gamma^{(001)_{Ar}/(00.1)_{Cc}}_{int}$) Energies (erg cm^{-2}) for the $(001)_{Ar}/(00.1)_{Cc}$ Interface[a]

aragonite surface	calcite surface	$\gamma^{Ar}_{(001)}$	$\gamma^{Cc}_{(00.1)}$	$\beta^{(001)_{Ar}/(00.1)_{Cc}}_{adh}$	$\gamma^{(001)_{Ar}/(00.1)_{Cc}}_{int}$
$(001)^{Ar}_{CO_3}$	$(00.1)^{Cc}_{Ca}$	779	834	464	1149
	$(00.1)^{Cc}_{CO_3}$		764	1249	294

[a]Surface energies of the (001) and (00.1) faces of aragonite ($\gamma^{Ar}_{(001)}$) and calcite ($\gamma^{Cc}_{(00.1)}$), respectively, are also reported.

The difference between the two specific adhesion energy values (Table 4) and, consequently, between the values of the two specific energies is striking. The calcite surface profile $(00.1)^{Cc}_{CO_3}$ is largely favored for the $(001)_{Ar}/(00.1)_{Cc}$ epitaxy to occur. Moreover, the corresponding adhesion energy (1249 erg cm^{-2}) is so high that the interface energy value (294 erg cm^{-2}) of the $(001)_{Ar}/(00.1)_{Cc}$ epitaxial interface is reduced by 61 and 62% with respect to those of the "free surfaces" of aragonite and calcite, respectively. However, this is not the only amazing property of this epi-interface, as it will be shown in the following section. Optimized and not optimized $(001)_{Ar}/(00.1)_{Cc}$ interface structures generated with the $(00.1)^{Cc}_{CO_3}$ surface are reported in Figure 2, whereas those obtained with the $(00.1)^{Cc}_{Ca}$ surface are drawn in Figure S1 (Supporting Information).

3.1.2. New $CaCO_3$ Polymorph Associated with the Low-Temperature Transition: $(001)_{Ar} \leftrightarrow (00.1)_{Cc}$. When analyzing the optimized structure of the $(001)_{Ar}/(00.1)_{Cc}$ composed slab, we obtained an unexpected result, the original structure of the $(001)_{Ar}$ slab (Figure 2a) is strongly modified to such an extent that a different stabilized phase does set up at the contact with the (00.1) surface of calcite (Figure 2b). We extracted from the new slab structure its unit cell (Figure 2b) and determined the corresponding space group (SG; $P6_322$) and the asymmetric unit using the FINDSYM[31] program. Successively, an optimization of the bulk structure (always at the empirical level) in the space group $P6_322$, was carried out, and cell parameters and atomic fractional coordinates are listed in Table S2 (Supporting Information), along with those of calcite and aragonite, for comparison. Surprisingly, the computationally predicted $CaCO_3$ polymorph spontaneously generates at the $(001)_{Ar}/(00.1)_{Cc}$ interface and at low temperature (0 K), is the same as that already obtained by other researchers, when studying the high-temperature aragonite−calcite breakdown by means of both empirical[32,33] and quantum-mechanical simulations.[34] In particular, Gavryushkin et al.,[34] through molecular dynamics simulation at the quantum-mechanical level and evolutionary metadynamic calculations, found that the aragonite structure was stable up to 700−800 K. At 800 K, the new phase with hexagonal symmetry was formed and was stable up to 1000 K; this hexagonal $CaCO_3$ polymorph was named hexarag (hAr). Instead, at an empirical level, depending on the potential used the phase transition from aragonite to hexarag has been fixed at 500[33] and 1706 K,[32] respectively. To better characterize the transition temperature and transformation mechanism, we performed quantum-mechanical calculations at the DFT level (computational details are given in the Supporting Information) and noticed that, as the volume of the aragonite unit cell increases due to the increasing temperature, its static energy increases as well, until it intersects the curve representing the hexarag energy (Figure 3). The intersection occurs at a cell volume of ∼242 Å^3, corresponding to the transition temperature of ∼600 K. The aragonite−hexarag transition is driven by a soft mode, and no activation energy is needed. The frequency of the A_u vibrational (soft) mode corresponding to rigid rotations of the carbonate groups in the (001) plane tends to zero as the volume of aragonite increases; the mode becomes increasingly anharmonic and, at a given volume, the computed harmonic frequency becomes an imaginary number, thus signaling the intrinsic instability of the structure in the space group *Pmcn*. The equilibrium volume of hexarag is higher than that of aragonite. Instead, calcite has an equilibrium volume that is not too far from the equilibrium volume of the hexarag, but it has an energy, which is significantly lower than the latter.

As previously obtained by Gavryushkin et al.,[34] we computed the phonon spectrum of hexarag both at empirical and quantum-mechanical levels. Ab initio frequencies are listed in the Supporting Information. No imaginary frequencies were obtained, thus confirming that hexarag has a stable minimum energy structure and it can exist as a crystalline phase; hence, it does not represent a transition state.

Hexarag is a non-centrosymmetric phase belonging to the hexagonal system (point group 622) which shows some structural analogies with calcite: in both phases, alternating layers of Ca^{2+} and CO_3^{2-} ions are stacked along [001]; CO_3^{2-} ions have the same orientation in a single layer, but they are rotated by 30° in the successive one. However, unlike calcite, successive layers of CO_3^{2-} ions are perfectly superimposed. Consequently, hexarag is found to have a density of 2.70 g cm^{-3}, almost the same as that of calcite (2.71 g cm^{-3}).[35]

This kind of behavior is peculiar in the epitaxially mediated transitions between two crystal phases. In the following sections

https://doi.org/10.1021/acs.jpcc.2c00785
J. Phys. Chem. C 2022, 126, 6472−6481

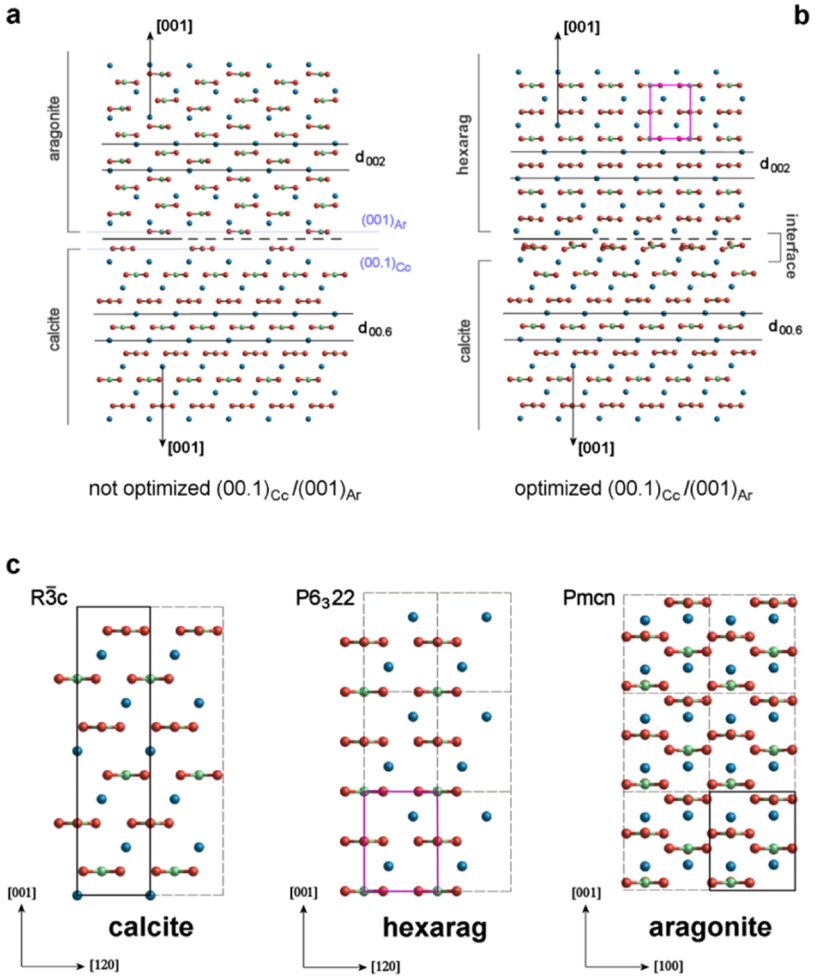

Figure 2. Formation of the hexagonal $CaCO_3$ polymorph at the epitaxial contact with calcite. (a) $(00.1)_{Cc}/(001)_{Ar}$ composed slab before geometry optimization; Ca is blue, C is green, and O is red. (b) $(00.1)_{Cc}/(001)_{Ar}$ composed slab after geometry optimization; the formation of a new phase in place of aragonite is evident: the unit cell of hexarag is drawn (violet solid line). (c) Bulk structure of hexarag is drawn, along with those of calcite and aragonite, for comparison.

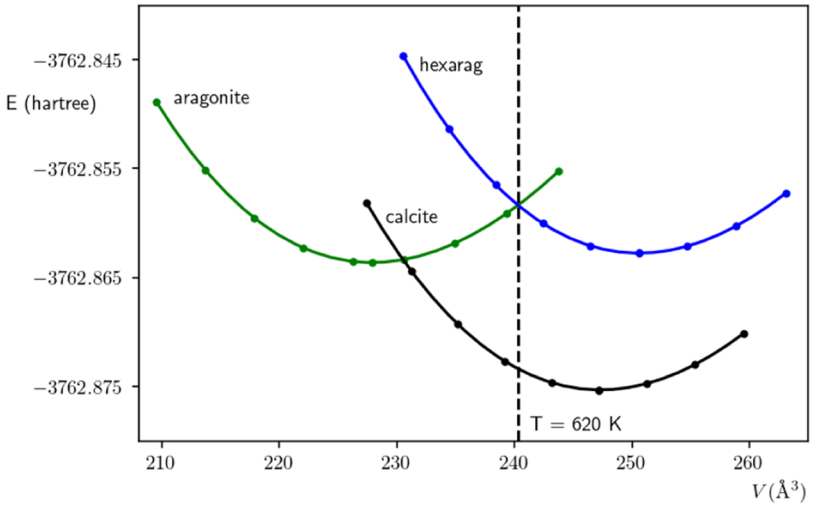

Figure 3. Static energy vs cell volume of calcite, aragonite, and hexarag. From the computed (this work) thermal expansion of aragonite, it can be estimated that the volume at which the latter phase (green curve) becomes intrinsically unstable, and transforms into the $P6_322$ hexarag, corresponds to a temperature of 620 K. After the soft-mode driven transition, at zero pressure, the structure of hexarag (blue curve) relaxes to an equilibrium volume slightly larger than that of calcite (black curve).

we will investigate if the remaining aragonite/calcite epitaxies confirm the uniqueness or not of the $(001)_{Ar}/(00.1)_{Cc}$ epitaxy.

To verify that the hexarag formation is not a computational artifact due to the size of the considered system, we performed

https://doi.org/10.1021/acs.jpcc.2c00785
J. Phys. Chem. C 2022, 126, 6472−6481

Table 5. Main 2D-Coincidence Lattices Describing the $(100)_{Ar}/(11.0)_{Cc}$ Epitaxy[a]

		$(100)_{Ar}$	$(11.0)_{Cc}$	linear and area misfit (%)	notes
	ranking				
2D-cell corresponding lattice vectors (Å)	(1)	3[001] = 17.246	[001] = 17.06	−1.09	rectangular 2D-supercell
		[010] = 7.9672	$[1\bar{1}0]$ = 8.6422	+8.47	
2D-supercell area (Å^2) and multiplicity		137.403 (3×)	147.436 (1×)	+7.30	parallel crystals
2D-cell corresponding lattice vectors (Å)	(2)	2[010] = 15.9344	[001] = 17.06	+7.06	rectangular 2D-supercell
		3[001] = 17.246	$2[\bar{1}10]$ = 17.284	+0.22	
2D-supercell area (Å^2) and multiplicity		274.806 (6×)	294.872 (2×)	+7.30	orthogonal crystals

[a]Parallel crystals mean that the parameters c have the same direction in both crystals, while in the orthogonal crystals the same parameters are placed at 90° from the other.

the calculations by increasing the size of the $(00.1)_{Cc}$ and $(001)_{Ar}$ slabs, until the GULP program allowed us to do it; beyond a certain number of atoms it was not possible to solve a memory allocation problem in GULP. It is interesting to note that we always observed the formation of hexarag, irrespective of the thickness of the slabs considered. Hence, the hexarag formation in adhesion on calcite is not a computational artifact.

Moreover, we also calculated the dipole moment perpendicular to the composed slab with increasing thickness. The thickest composed slab we used in our calculations is formed by 30 d_{002}-layers of aragonite and 31 d_{006}-layers of calcite and has a macroscopic dipole moment of 0.2120 eÅ. Instead, a composed slab formed by 25 d_{002}-layers of aragonite and 24 d_{006}-layers of calcite has a macroscopic dipole moment of 0.1976 eÅ. A slightly increasing dipole moment is observed with increasing slab thickness.

3.2. Aragonite (100)/Calcite (11.0) Epitaxy. The pinacoid {100} of aragonite shows a sharp stepped (S) character because in the elementary slices of thickness d_{200}, imposed by the extinction rules, no bond can be found between adjacent [001] PBCs in the first coordination sphere. The surface energy of the (100) face is $\gamma^{Ar}_{(100)}$ = 1028 erg cm^{-2}.[28] $\{100\}_{Ar}$ does not appear, neither in the theoretical equilibrium[26−30] form nor on the growth shape of the crystal;[27] furthermore, it is practically never observed in both nature and lab.[27]

The character of the hexagonal {11.0} prism of calcite is definitely flat (F).[36,37] Along with the cleavage rhombohedron {10.4} it is the most compact calcite form; accordingly, its surface energy value is $\gamma^{Cc}_{(11.0)}$ = 1232 erg cm^{-2}. Despite its fairly low surface energy, the {11.0} form does not enter the theoretical (in the vacuum, at 0 K) equilibrium form of the crystal, owing to the competition with the other prism {10.0} in the [001] calcite zone, as we will see later. Despite all this, the $(100)_{Ar}/(11.0)_{Cc}$ epitaxy does deeply modify the theoretical equilibrium form of both calcite and aragonite, owing to its structural and energetic features.

In Table 5, the main 2D-coincidence lattices considered to describe the $(100)_{Ar}/(11.0)_{Cc}$ epitaxy are listed. Complete description of 2D-coincidence lattices can be seen in Table S3 (Supporting Information). Ranking increases with the size of the 2D-supercell area.

A preliminary comment concerns ranking (1) of Table 5, where aragonite and calcite crystals are parallel to each other, their [001] directions being coincident. The view along the common [001] direction shows mutual relations on their lattice planes $(001)_{Ar}$ and $(00.1)_{Cc}$. This finding proves that from the coupling of the $(100)_{Ar}/(11.0)_{Cc}$ faces, elementary lamellae can cross, during growth, the frontier between the two crystals, owing to the fact that the thickness of the two slices d_{002} of aragonite and d_{006} of calcite are practically the same.

Our results propose a new way of thinking about the transition between two crystal phases. The interface is not an ideal lattice plane, but the place where the intergrowth can occur, if the epitaxial constraints are fulfilled.

As to ranking (2) of Table 5, the situation is fully different. $[001]_{Cc}$ is orthogonal to the $[001]_{Ar}$ and, accordingly, the carbonate groups become perpendicular to each other when crossing the interface between the two individuals. As a consequence, the epitaxy can hardly occur, although reticular conditions would be favorable in themselves. For this reason, we decided not to calculate the energies associated with ranking (2).

3.2.1. Energetics of the $(100)_{Ar}/(11.0)_{Cc}$ Epitaxy. The adhesion and interface energies related to the epitaxy defined by the 2D cell with ranking (1), are $\beta^{(100)_{Ar}/(11.0)_{Cc}}_{adh}$ = 1547 erg cm^{-2} and $\gamma^{(100)_{Ar}/(11.0)_{Cc}}_{int}$ = 713 erg cm^{-2}, respectively. They are calculated by considering the following surface energies: $\gamma^{Ar}_{(100)}$ = 1028 and $\gamma^{Cc}_{(11.0)}$ = 1232 erg cm^{-2}.

This adhesion energy value is ∼24% higher than that of the $(001)_{Ar}/(00.1)_{Cc}$ epitaxy and, consequently, the epi-interface $(100)_{Ar}/(11.0)_{Cc}$ is largely favored with respect to both aragonite and calcite "free" interfaces, respectively. Such behavior could affect the theoretical equilibrium shape of both crystals, as we have already pointed out when dealing with the $(001)_{Ar}/(00.1)_{Cc}$ epitaxy. Optimized and not optimized $(100)_{Ar}/(11.0)_{Cc}$ interface structures are reported in Figure S2 (Supporting Information). Interestingly, the slab $(001)_{Ar}$ is only partly transformed into hexarag where slices of aragonite alternate with slices of hexarag.

3.3. Aragonite(110)/Calcite(10.0) Epitaxy. The {110} prism of aragonite shows a sharp F character[27,28] and its elementary d_{110} slices can exhibit two possible surface profiles: the simplest one, terminated by Ca^{2+} ions does not need to be reconstructed, unlike the second one, which is CO_3^{2-} terminated, since the carbonate ions are shared by two adjacent and successive slices. The Ca^{2+} terminated slices have a specific surface energy of 730 erg cm^{-2} while for the CO_3^{2-} terminated slices it is 797 erg cm^{-2}.

The {10.0} prism of calcite has a marked stepped (S) character, owing to the fact that the extinction rules of the space group of calcite impose an elementary slice of thickness d_{300} within which no bond can be found among the contiguous [001] PBCs.[37] Accordingly, its surface energy is a very moderate value of $\gamma^{Cc}_{(10.0)}$ = 722 erg cm^{-2}, which is surprising for a stepped face. For reasons of conciseness, we illustrate in Table 6 only the 2D-coincidence lattice that was adopted for the energy calculation concerning the coupling: $(110)_{Ar}/(10.0)_{Cc}$. The list of complete 2D-coincidences is reported in Table S4 (Supporting Information).

The situation shown in this Table 6 is very interesting, the best match between the lattices of the two prisms developing along

https://doi.org/10.1021/acs.jpcc.2c00785
J. Phys. Chem. C 2022, 126, 6472−6481

Table 6. Main 2D-Coincidence Lattice Describing the $(110)_{Ar}/(10.0)_{Cc}$ Epitaxy. No angular misfit exists between the corresponding vectors defining the 2D-coincidence cell

	$(110)_{Ar}$	$(10.0)_{Cc}$	linear and area misfit (%)
2D-cell corresponding lattice vectors (Å)	3[001] = 17.2212	[001] = 17.0600	−0.945
	$[\bar{1}10]$ = 9.3855	2[010] = 9.9792	+6.32
2D-supercell area (Å^2) and multiplicity	161.6295 (3×)	170.245 (2×)	+5.33

the common z-axes, $(110)_{Ar}$ and $(10.0)_{Cc}$, corresponds to strategic features of the two crystal species:

(i) 110 is the original composition plane of the well-known (110) twin law of aragonite. In the coupling aragonite/calcite, the form $\{110\}_{Ar}$ transforms into a substrate on which calcite can epitaxially nucleate, forming a fourfold interface $(110)_{Ar}/(10.0)_{Cc}$. Linear misfits are opposite to each other, and then, the area misfit (5.33%) is small also because the angular misfit does not exist.

(ii) The coincidence along the z-axes of the two structures is astonishing, as a matter of fact, the misfit between $3[001]_{Ar}$ and $[001]_{Cc}$ is lower than 1%. In other words, the stacking of the elementary growth layers, along the z-axis, does not change when going from aragonite to calcite, as follows when considering d_{002} = 2.8702 Å for aragonite, while d_{006} = 2.8433 Å for calcite. This means that these elementary layers do perfectly face each other at the interface generated by the epitaxial contact.

(iii) Summing up, the final aspect of this epi-growth is an aggregate made by a prismatic single crystal of calcite (guest) developing parallel to a prismatic single crystal of aragonite (host). In both crystals, the planar CO_3^{2-} ions are rigorously perpendicular to their respective z-axes.

3.3.1. Energetics of the $(110)_{Ar}/(10.0)_{Cc}$ Epitaxy. The just exposed considerations should be in favor of a good $(110)_{Ar}/(10.0)_{Cc}$ epitaxy. Nonetheless, the related adhesion energy is rather modest, $\beta_{adh}^{(110)_{Ar}/(10.0)_{Cc}}$ = 131 erg cm^{-2}. Consequently, the corresponding interfacial energy, $\gamma_{int}^{(110)_{Ar}/(10.0)_{Cc}}$ = 1321 erg cm^{-2}, largely exceeds the values of both the specific surface energy values $\gamma_{(110)}^{Ar}$ = 730 erg cm^{-2} (Ca-terminated) and $\gamma_{(10.0)}^{Cc}$ = 722 erg cm^{-2} of the involved free surfaces, which makes the realization of such an epitaxial event extremely difficult. The only reason we can give to explain this contradiction between geometry and energy, is related to the relative orientation of the triangular carbonate ions in the transition from aragonite to calcite. As a matter of fact, when crossing the aragonite/calcite interface, a sharp discontinuity does occur, since the [001] carbonate rows rotate 30°, placing the two structures in "phase opposition" (Figure S3a, Supporting Information). In this epitaxy, the phase opposition that implies weak attraction between facing [001] carbonate rows has a periodicity of ∼5 Å along the parallel directions $[010]_{Cc}/[\bar{1}10]_{Ar}$. The same "phase opposition" occurs as well in the just investigated $(100)_{Ar}/(11.0)_{Cc}$ epitaxy, but its associated periodicity increases to ∼8 Å along the parallel directions $[\bar{1}10]_{Cc}/[010]_{Ar}$. This could be a sensible structural reason to explain why the value (131 erg cm^{-2}) of the adhesion energy for the $(110)_{Ar}/(10.0)_{Cc}$ epitaxy is so low with respect to the one (1547 erg cm^{-2}) obtained for the $(100)_{Ar}/(11.0)_{Cc}$ epitaxy. Optimized and not optimized $(110)_{Ar}/(10.0)_{Cc}$ interface structures are reported in Figure S3 (Supporting Information).

This last consideration allows us to underline once more that good 2D-lattice coincidences constitute a necessary, but not sufficient, condition for an epitaxy could occur. Structural continuity between the facing crystal phases is needed as well, as proved by the value of the adhesion energy.

3.4. Aragonite(010)/Calcite(01.2) Epitaxy. The {010} pinacoid of aragonite shows a sharp F character[27,28] and its elementary d_{010} slices can exhibit two possible surface profiles: one is terminated by Ca^{2+} ions and the other one is CO_3^{2-} terminated; both terminations do not need reconstruction. The Ca^{2+} terminated surface has a specific surface energy of 808 erg cm^{-2}, while for the CO_3^{2-} terminated surface it is 868 erg cm^{-2}.

The {01.2} rombohedron of calcite is a flat (F) form.[38] When it is observed along the [100] direction, the (01.2) face is composed of alternating layers of Ca^{2+} ions and CO_3^{2-} groups and, as a consequence, such a face is a dipolar one and shows unstable terminations that need to be reconstructed. Several reconstructions can be performed to stabilize the (01.2) face,[38] but here we only considered that on giving the lowest surface energy half of the outmost charged layer is removed, like the R1 reconstruction described for $(00.1)_{Cc}$. Accordingly, two (01.2) terminations are allowed: Ca^{2+} terminated and CO_3^{2-} terminated having specific surface energies of 1040 and 750 erg cm^{-2}, respectively.

In Table 7, the 2D-coincidence lattice that we adopted for the energy calculation of the coupling $(010)_{Ar}/(0.12)_{Cc}$ is reported. The list of complete 2D-coincidences is reported in Table S5 (Supporting Information).

3.4.1. Energetics of the $(010)_{Ar}/(01.2)_{Cc}$ Epitaxy. We calculated the adhesion energy, $\beta_{adh}^{(010)_{Ar}/(01.2)_{Cc}}$, for two epitaxial interfaces obtained by combining the Ca^{2+} terminated $(010)_{Ar}$ with (i) the Ca^{2+} terminated $(01.2)_{Cc}$ and (ii) the CO_3^{2-} terminated $(01.2)_{Cc}$. Interestingly, $\beta_{adh}^{(010)_{Ar}/(01.2)_{Cc}}$ for interfaces (i) and (ii) are 297 and −558 erg cm^{-2}, respectively. A negative value means that there is repulsion between aragonite and calcite, and the interface cannot form. Therefore, only interface (i) is physically meaningful, despite the very low value of the adhesion energy and, consequently, a high interfacial energy, $\gamma_{int}^{(010)_{Ar}/(01.2)_{Cc}}$ = 1551 erg cm^{-2}, which largely exceeds the values of both the specific surface energy values $\gamma_{(010)}^{Ar}$ = 808 erg cm^{-2} (Ca^{2+} terminated) and $\gamma_{(01.2)}^{Cc}$ = 750 erg cm^{-2} (CO_3^{2-} terminated) of the involved free surfaces, making the realization of such an epitaxial event extremely difficult.

The low adhesion energy is a consequence of the different structural arrangement of the CO_3^{2-} groups at the $(010)_{Ar}/(01.2)_{Cc}$ interface, as it is possible to see in Figure S4 (Supporting Information), where optimized and not optimized

Table 7. Main 2D-Coincidence Lattice Describing the $(010)_{Ar}/(01.2)_{Cc}$ Epitaxy

	$(010)_{Ar}$	$(01.2)_{Cc}$	linear and area misfit (%)	notes
2D-cell corresponding lattice vectors (Å)	$[\bar{3}0\bar{1}]$ = 15.952	1/3 $[\bar{4}4\bar{2}]$ = 16.199	+1.55	rectangular 2D-supercell
	$[\bar{1}02]$ = 12.5074	1/3 $[5\bar{2}1]$ = 11.844	−5.56	
2D-supercell area (Å^2) and multiplicity	199.36 (7×)	190.998 (6×)	−4.37	

https://doi.org/10.1021/acs.jpcc.2c00785
J. Phys. Chem. C 2022, 126, 6472−6481

interface structures are reported. There is not a good structural continuity when moving from aragonite to calcite, the CO_3^{2-} groups in calcite being strongly tilted and rotated with respect to those in aragonite.

4. CONCLUSIONS

To establish the most likely epitaxial relationships between calcite (Cc) and aragonite (Ar), here we investigated at the empirical level the $(001)_{Ar}/(00.1)_{Cc}$, $(110)_{Ar}/(10.0)_{Cc}$, $(010)_{Ar}/(01.2)_{Cc}$, and $(100)_{Ar}/(11.0)_{Cc}$ interfaces. From the analysis of the optimized structure of the $(001)_{Ar}/(00.1)_{Cc}$ composed slab, we obtained an unexpected result: the original structure of the $(001)_{Ar}$ slab was strongly modified to such an extent that a different stabilized phase (hexarag) was set up at the contact with the (00.1) surface of calcite.

The exceptional nature of this finding lies in the identification of a hexagonal $CaCO_3$ polymorph forming both at high temperature, within the aragonite−calcite transition, and at room temperature, in epitaxy with calcite. In particular, hexarag forms only at the peculiar $(001)_{Ar}/(00.1)_{Cc}$ interface. For the other investigated interfaces, original aragonite structure was not or slightly modified by adhesion with calcite.

Another interesting feature of the $(001)_{Ar}/(00.1)_{Cc}$ interface concerns its energetics. A very high adhesion energy was calculated, $\beta_{adh}^{(001)_{Ar}/(00.1)_{Cc}} = 1249$ erg cm^{-2}, thus yielding a very low interface energy, $\gamma_{int}^{(001)_{Ar}/(00.1)_{Cc}} = 294$ erg cm^{-2}. This energy is significantly lower with respect to those of the other calcite/aragonite interfaces studied (713−1551 erg cm^{-2}), in which the hexagonal phase did not develop. Moreover, it should be remembered that in the cases we studied, all of the 3D aragonite−calcite transitions occur at supersaturation and that supersaturation lowers as much as the epitaxy improves the quality of the adhesion.

On this ground, we can try to explain why some mollusks and gastropods develop a layer of calcite in the outer portion of their shell, while others do not. It should be highly probable that only the organisms producing a columnar or fibrous layer of aragonite with the *c*-axis perpendicular to the lamination of the underlying nacre and crystal morphology with the {001} form exposed to the seawater are able to generate calcite (Figure 4). Indeed, the flat {001} form of aragonite promotes the nucleation of calcite, through the generation of an intermediate phase (hexarag), which modifies the structure of the interface. The resulting adhesion energy increases (so the interface energy is lowered) and calcite is allowed to nucleate, even at low supersaturations. Then, hexarag works as a buffer between calcite and aragonite, at room temperature (activation of ΔG for nucleation does not intervene, the temperature effect being not required). Further, it is worth recollecting that the structure of this nanocrystalline buffer is not centrosymmetric ($P6_322$) and is intermediate, not by chance, between a decidedly lower symmetric (aragonite, *Pmcn*) and a higher symmetric phase (calcite, $R\bar{3}c$), both of which are centrosymmetric. Hexarag develops only through specific crystallographic planes and its formation requires that *c*-axes of calcite and aragonite should be parallel. In fact, such topotaxial relationship has already been discussed in geological samples.[5,11] Here, we propose that (bio)minerals displaying calcite and aragonite in epitaxial contact are candidates for finding hexarag. We hypothesize that this polymorph occurs on the nanoscale in an intimate structural relationship with calcite and aragonite, therefore, we suggest the use of TEM for its identification.

Recently, just using TEM, another nanocrystalline $CaCO_3$ polymorph (mAra) was detected[39] in the first carbonate precipitates occurring in a cold cave decorated by aragonite speleothems. It is a monoclinic phase ($P2_1/c$) with structure and density (~3 g cm^{-3}) similar to those of aragonite. According to the authors, this phase does occur before the usual orthorhombic aragonite and plays a key role in metastable aragonite formation.

The discovery of these two $CaCO_3$ polymorphs suggests a more careful observation of $CaCO_3$ phases at the nanoscale. In particular, the formation of the hexagonal polymorph at the calcite/aragonite interface, exclusively described until now in the high-temperature polymorphic transformation, clearly outlines the importance of intensifying the study of the transition zone (i.e., the nanometer-sized diffuse interface) that should occur when two phases are placed in reticular contact that fulfils the epitaxial constraints. Such a study must be conducted at both theoretical (e.g., 2D composed slab simulations) and experimental levels, to gain not only structural information but also to determine those thermodynamic quantities that are needed to establish the formation mechanism of the phases involved in the epitaxy.

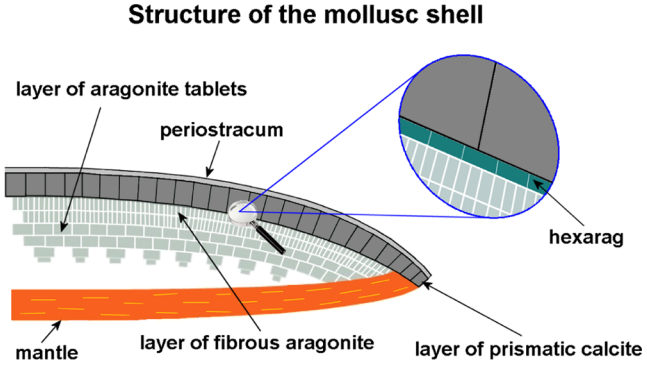

Figure 4. Schematic structure of the mollusk shell. From the inner (mantle) to the outer of the shell (periostracum, which is composed of chitin), one observes: (i) a nacreous layer formed by the (001) pseudohexagonal tablets of aragonite, with the *c*-axis of the tablets perpendicular to the lamination of nacre; (ii) a fibrous layer of aragonite crystals, in which in the upper part of this layer, the *c*-axis of the aragonite crystals are perpendicular to the shell surface; and (iii) a nanolayer of hexarag which works as a buffer between aragonite and (iv) a layer of prismatic calcite.

■ ASSOCIATED CONTENT

Supporting Information

The Supporting Information is available free of charge at https://pubs.acs.org/doi/10.1021/acs.jpcc.2c00785.

Table S1: 2D-coincidence lattices describing the $(001)_{Ar}/(00.1)_{Cc}$ epitaxy, Table S2: cell parameters and fractional coordinates of hexarag, aragonite, and calcite, Table S3: the 2D-coincidence lattices describing the $(100)_{Ar}/(11.0)_{Cc}$ epitaxy, Table S4: the main 2D-coincidence lattices describing the $(110)_{Ar}/(10.0)_{Cc}$ epitaxy, Table S5: the main 2D-coincidence lattices describing $(010)_{Ar}/(01.2)_{Cc}$ epitaxy, computational details; Figure S1: optimized and not optimized structures of the $(00.1)_{Cc}/(001)_{Ar}$ interface, Figure S2: optimized and not optimized structures of the $(11.0)_{Cc}/(100)_{Ar}$ interface, Figure S3: optimized and not optimized structures of the $(10.0)_{Cc}/$

https://doi.org/10.1021/acs.jpcc.2c00785
J. Phys. Chem. C 2022, 126, 6472−6481

$(110)_{Ar}$ interface, Figure S4: optimized and not optimized structures of the $(01.2)_{Cc}/(010)_{Ar}$ interface (PDF)

AUTHOR INFORMATION

Corresponding Author

Marco Bruno − *Dipartimento di Scienze della Terra, Università degli Studi di Torino, 10125 Torino (TO), Italy; SpectraLab s.r.l., Spin-off accademico dell'Università degli Studi di Torino, 10135 Torino (TO), Italy; NIS, Centre for Nanostructured Interfaces and Surfaces, Università degli Studi di Torino, 10135 Torino (TO), Italy;* orcid.org/0000-0002-0161-574X; Email: marco.bruno@unito.it

Authors

Mauro Prencipe − *Dipartimento di Scienze della Terra, Università degli Studi di Torino, 10125 Torino (TO), Italy; NIS, Centre for Nanostructured Interfaces and Surfaces, Università degli Studi di Torino, 10135 Torino (TO), Italy;* orcid.org/0000-0003-3958-1888

Dino Aquilano − *Dipartimento di Scienze della Terra, Università degli Studi di Torino, 10125 Torino (TO), Italy;* orcid.org/0000-0002-3908-928X

Andrea Cotellucci − *Dipartimento di Scienze della Terra, Università degli Studi di Torino, 10125 Torino (TO), Italy*

Stefano Ghignone − *Dipartimento di Scienze della Terra, Università degli Studi di Torino, 10125 Torino (TO), Italy*

Péter Németh − *Institute for Geological and Geochemical Research, Research Centre for Astronomy and Earth Sciences, Eötvös Loránd Research Network, 1112 Budapest, Hungary; Research Institute of Biomolecular and Chemical Engineering, Nanolab, University of Pannonia, 8200 Veszprém, Hungary*

Complete contact information is available at: https://pubs.acs.org/10.1021/acs.jpcc.2c00785

Notes

The authors declare no competing financial interest.

ACKNOWLEDGMENTS

The present study has been partly funded by the project PRIN 2017 (2017L83S77) of the Italian Ministry for Education, University and Research (MIUR). PN acknowledges support from the Ministry of Innovation and Technology of Hungary from the National Research, Development and Innovation Fund (projects FK141842 and ANN141894).

REFERENCES

(1) Faust, G. T. Differentiation of Aragonite from Calcite by Differential Thermal Analysis. *Science* **1949**, *110*, 402−403.

(2) Faust, G. T. Thermal analysis studies on carbonates. I Aragonite and calcite. *Am. Mineral.* **1950**, *35*, 207−224.

(3) Gruver, R. M. Differential Thermal-Analysis Studies of Ceramic Materials: II, Transition of Aragonite to Calcite. *J. Am. Ceram. Soc.* **1950**, *33*, 171−174.

(4) Kleber, W. Neues Jahr *Min. (A)* 1940, *75*, 465 480.

(5) Dasgupta, D. R. The oriented transformation of aragonite into calcite. *Mineral. Mag. J. Mineral. Soc.* **1964**, *33*, 924−928.

(6) Bischoff, J. L.; Fyfe, W. S. Catalysis, inhibition, and the calcite-aragonite problem. I. The aragonite-calcite transformation. *Am. J. Sci.* **1968**, *266*, 65−79.

(7) Brar, N. S.; Schloessin, H. H. Nucleation and growth of aragonite in calcite single crystal. *Phase Trans.* **1980**, *1*, 299−323.

(8) Carlson, W. D.; Rosenfeld, J. L. Optical determination of topotactic aragonite-calcite growth kinetics: metamorphic implications. *J. Geol.* **1981**, *89*, 615−638.

(9) Gillet, P.; Madon, M. Un modèle de dislocations pour la transition aragonite ↔ calcite. *Bull. Mineral.* **1982**, *105*, 590−597.

(10) Madon, M.; Gillet, P. A theoretical approach to kinetics of calcite ↔ aragonite transition: application to laboratory experiments. *Earth Planet. Sci. Lett.* **1984**, *67*, 400−414.

(11) Bruni Frisia, S.; Wenk, H. R. Replacement of aragonite by calcite in sediments from the San Cassiano formation (Italy). *J. Sediment. Petrol.* **1985**, *55*, 159−170.

(12) Frisia, S.; Borsato, A.; Hellstrom, J. High spatial resolution investigation of nucleation, growth and early diagenesis in speleothems as exemplar for sedimentary carbonates. *Earth-Sci. Rev.* **2018**, *178*, 68−91.

(13) Mann, S. *Biomineralitazion, Principles and Concepts in Bioinorganic Materials Chemistry*; Oxford University Press: New York, 2001.

(14) Wada, K. Crystal growth of molluscan shells. *Bull. Nat. Pearl Res. Lab.* **1961**, *7*, 703−828.

(15) Wise, S. W., Jr. Microarchitecture and deposition of gastropod nacre. *Science* **1970**, *167*, 1486−1488.

(16) Checa, A. G.; Rodriguez-Navarro, A. B. Self-organisation of nacre in the shells of Pterioida (Bivalvia: Mollusca). *Biomaterials* **2005**, *26*, 1071−1079.

(17) Dauphin, Y.; Ball, A. D.; Cotte, M.; Cuif, J. P.; Meibom, A.; Salomé, M.; Susini, J.; Williams, C. T. Structure and composition of the nacre-prisms transition in the shell of Pinctada margaritifera (Mollusca, Bivalvia). *Anal. Bioanal. Chem.* **2008**, *390*, 1659−1669.

(18) Bruno, M.; Rubbo, M.; Pastero, L.; Massaro, F. R.; Nestola, F.; Aquilano, D. Computational approach to the study of epitaxy: natural occurrence in diamond/olivine and aragonite/zabuyelite. *Cryst. Growth Des.* **2015**, *15*, 2979−2987.

(19) Bruno, M.; Massaro, F. R.; Rubbo, M. A new computational approach to the study of epitaxy: the calcite/dolomite case. *CrystEngComm* **2017**, *19*, 3939−3946.

(20) Rohl, A. L.; Wright, K.; Gale, J. D. Evidence from surface phonons for the (2×1) reconstruction of the $(10\bar{1}4)$ surface of calcite from computer simulation. *Am. Mineral* **2003**, *88*, 921−925.

(21) Gale, J. D. GULP: A computer program for the symmetry-adapted simulation of solids. *J. Chem. Soc., Faraday Trans.* **1997**, *93*, 629−637.

(22) Bruno, M.; Prencipe, M. A new calculation strategy to analyze the vibrational free energy of a slab and calculate the vibrational contribution of the surface free energy. *CrystEngComm* **2013**, *15*, 6736−6744.

(23) Bruno, M. The free energy density of a crystal: calcite ($CaCO_3$) as a case of study. *CrystEngComm* **2015**, *17*, 2204−2211.

(24) Kern, R. Croissance épitaxique (aspects topologiques et structuraux). *Bull. Mineral.* **1978**, *101*, 202−233.

(25) Hartman, P.; Perdok, W. G. On the relations between structure and morphology of crystals. I. *Acta Crystallogr.* **1955**, *8*, 49−52.

(26) Heijnen, W. M. M. Neues Jahrb *Mineral. Abh.* 1986, *154*, 223 245.

(27) Aquilano, D.; Rubbo, M.; Catti, M.; Pavese, A. Pavese Theoretical equilibrium and growth morphology of $CaCO_3$ polymorphs I. Aragonite. *J. Cryst. Growth* **1997**, *182*, 168−184.

(28) Massaro, F. R.; Bruno, M.; Rubbo, M. Surface structure, morphology anf (110) twin of aragonite. *CrystEngComm* **2014**, *16*, 627−635.

(29) Heijnen, W. M. M. The morphology of gel grown calcite. *Neues Jahrb. Miner. Mh.* **1985**, *8*, 357−371.

(30) Bruno, M.; Prencipe, M.; Massaro, F. R.; Aquilano, D. Surface reconstructions and relaxation effects in a centre-symmetrical crystal: the {00.1} form of calcite ($CaCO_3$). *CrystEngComm* **2010**, *12*, 3626−3633.

(31) Stokes, H. T.; Hatch, D. M. FINDSYM: Program for identifying the space-group symmetry of a crystal. *J. Appl. Crystallogr.* **2005**, *38*, 237−238.

(32) Liu, J.; Ossowski, M.; Hardy, J.; Duan, C.-g.; Mei, W. Simulation of structural transformation in aragonite $CaCO_3$. *AIP Conf. Proc.* **2000**, *535*, 338−343.

(33) Miyake, A.; Kawano, J. High-temperature molecular dynamics simulation of aragonite. *J. Phys.: Condens. Matter* **2010**, *22*, No. 225402.
(34) Gavryushkin, P. N.; Belonoshko, A. B.; Sagatov, N.; Sagatova, D.; Zhitova, E.; Krzhizhanovskaya, M. G.; Rečnik, A.; Alexandrov, E. V.; Medrish, I. V.; Popov, Z. I.; et al. Metastable structures of $CaCO_3$ and their role in transformation of calcite to aragonite and postaragonite. *Cryst. Growth Des.* **2021**, *21*, 65−74.
(35) Markgraf, S. A.; Reeder, R. J. High-temperature structure refinements of calcite and magnesite. *Am. Mineral.* **1985**, *70*, 590−600.
(36) Aquilano, D.; Calleri, M.; Natoli, E.; Rubbo, M.; Sgualdino, G. The {1 0 4} cleavage rhombohedron of calcite: theoretical equilibrium properties. *Mater. Chem. Phys.* **2000**, *66*, 159−163.
(37) Roberto, M. F.; Bruno, M.; Aquilano, D. Effect of the Surface Relaxation on the Theoretical Equilibrium Shape of Calcite. 1. The [001] Zone. *Cryst. Growth Des.* **2010**, *10*, 4096−4100.
(38) Bruno, M.; Massaro, F. R.; Prencipe, M. Theoretical structure and surface energy of the reconstructed {01.2} form of calcite ($CaCO_3$) crystal. *Surf. Sci.* **2008**, *602*, 2774−2782.
(39) Németh, P.; Mugnaioli, E.; Gemmi, M.; Czuppon, G.; Demény, A.; Spötl, C. A nanocrystalline monoclinic CaCO3 precursor of metastable aragonite. *Sci. Adv.* **2018**, *4*, No. eaau6178.

https://doi.org/10.1021/acs.jpcc.2c00785
J. Phys. Chem. C 2022, 126, 6472−6481